

**ENVIRONMENTAL RESEARCH LETTERS****OPEN ACCESS****RECEIVED**  
27 January 2024**REVISED**  
6 June 2024**ACCEPTED FOR PUBLICATION**  
24 June 2024**PUBLISHED**  
5 July 2024

Original content from this work may be used under the terms of the [Creative Commons Attribution 4.0 licence](#).

Any further distribution of this work must maintain attribution to the author(s) and the title of the work, journal citation and DOI.

**LETTER**

# Decadal heatwave fluctuations in China caused by the Indian and Atlantic Oceans

Nan Lei<sup>1,2</sup> , Yongkun Xie<sup>1,\*</sup> , Zhongrui Bao<sup>1,2</sup>, Min Zhao<sup>1,2</sup>, Zifan Su<sup>1,2</sup> and Xiaodan Guan<sup>1,2</sup> <sup>1</sup> Collaborative Innovation Center for Western Ecological Safety, Lanzhou University, Lanzhou, People's Republic of China<sup>2</sup> College of Atmospheric Sciences, Lanzhou University, Lanzhou, People's Republic of China

\* Author to whom any correspondence should be addressed.

E-mail: [xieyk@lzu.edu.cn](mailto:xieyk@lzu.edu.cn)**Keywords:** heatwave, decadal fluctuation, China, Ocean, physical processSupplementary material for this article is available [online](#)**Abstract**

Heatwaves have been more common in China in recent years, largely attributed to human-caused global warming. While ocean variability, notably El Niño–Southern Oscillation (ENSO), influences regional heatwave fluctuations in China, the impact of other oceanic variability remains unclear. Here we show that the tropical Indian Ocean (TIO) and the tropical and subtropical North Atlantic Ocean (TSNAO) significantly modulate the decadal heatwave fluctuations in China. Among them, TIO has the most significant impact on northern China, while TSNAO has a greater impact on eastern China. TIO and TSNAO remotely influence heatwaves in China through abnormal sea surface temperatures (SSTs)-induced changes in atmospheric circulations involving westerlies and Rossby wave trains. Moreover, we demonstrated the physical processes responsible for heatwave fluctuations caused by TIO and TSNAO variability. The heatwave changes were determined jointly by vertical motion-related adiabatic and energy input-related diabatic temperature modifications. Our findings show that, in addition to ENSO, variability in the Indian and Atlantic Oceans is critical for understanding and predicting decadal heatwave changes in China.

## 1. Introduction

China has experienced severe heatwave events in recent years. For example, densely populated eastern China occurred persistent heatwaves in the summer of 2022, affecting some regions for over 2 months. Human-induced greenhouse gas emissions continuously raise global and regional temperatures to high levels, raising the occurrence of heatwaves as well (Sun *et al* 2017, Perkins-Kirkpatrick and Lewis 2020).

The occurrence of extreme heatwaves in China has a significant association with the westward extension or strengthening of the Western Pacific Subtropical High (WPSH) (Deng *et al* 2019, 2020, Liu *et al* 2019, Luo and Lau 2019, Cao *et al* 2022). The abnormal atmospheric circulation patterns are strongly linked to both local and remote sea surface temperature (SST) anomalies (Sun 2014, Cao *et al* 2022, Chen and Li 2023). Research has shown a significant association between the occurrence of heatwaves in China and anomalies in global SSTs,

with notable variations in the corresponding impacts across different regions of China (Wei *et al* 2020).

Sun (2014) documented that the unprecedented SST in the North Atlantic played a contributory role in generating anomalous East Asian upper-level westerlies and influencing the WPSH via teleconnection wave trains, resulting in extreme heatwaves in the Yangtze River of China in July 2013. Li *et al* (2015) proposed that tropical Indo-Pacific SST and their link to the associated behavior of WPSH were important in inducing extreme heat occurrences in Southern China during the summer of 2013.

Studies have revealed the factors influencing the heatwaves in China and pertinent SSTs (Chen and Li 2023, He *et al* 2023, Wang *et al* 2023, Zhang *et al* 2023). For example, He *et al* (2023) suggested the influence of the Tibetan Plateau on the tropical Indian Ocean SST. Wang *et al* (2023) emphasized the role of anomalous anticyclonic circulation in the mid-upper troposphere on heatwaves over central and eastern China. Notably, during the summer

of 2022, a sequence of consecutive climate phenomena occurred, including La Niña, a negative Indian Ocean dipole (IOD), and North Atlantic tripole SST patterns, which influenced the heatwaves in Eastern China (Jiang *et al* 2023). Wei *et al* (2023) demonstrated that El Niño–Southern Oscillation (ENSO), Atlantic Multidecadal Oscillation (AMO), and IOD explain 62.35% to 70.01% of the observed increase in heatwave intensity across different regions of China.

The component of decadal to multi-decadal climate changes that is modulated by internal climate variability is referred to as the decadal modulated oscillation (Huang *et al* 2017b). Atmospheric teleconnections play a crucial role in the decadal change in interannual variability in East Asia (Choi *et al* 2020). Research has already demonstrated that oceanic variability has played a significant role in slowing down global warming in the early 2000s (Kosaka and Xie 2013, Guan *et al* 2015, Fyfe *et al* 2016). Xie *et al* (2023a) also demonstrated a close correlation between decadal heatwaves from 1981 to 2017 in northern China and the Indo-Pacific warm pool and Northwest Pacific Ocean dipole during the early to mid-summer period.

However, the specific impacts of decadal oceanic variability on heatwaves in China remain unclear. Therefore, this study delineates a detailed analysis of the impact of SSTs in the tropical and subtropical North Atlantic Ocean (TSNAO) and tropical Indian Ocean (TIO) on the heatwaves in China. The underlying physical mechanisms were also demonstrated.

## 2. Data and methods

### 2.1. Data

The observational three-hourly and monthly near-surface air temperature data are from the European Center for Medium Weather Forecasting (ECMWF) reanalysis, version 5 (ERA5) in a  $1^\circ \times 1^\circ$  grid. The monthly geopotential of the atmosphere is from the ERA5 pressure-level dataset, in a  $1^\circ \times 1^\circ$  grid. The three-hourly temperature, zonal and meridional wind velocity, and vertical velocity in the pressure framework of the atmosphere are from the ERA5 model-level dataset, in a  $2^\circ \times 2^\circ$  grid (Hersbach *et al* 2020). The ERA5 data are available from 1940 to the present. The monthly SST is sourced from the Extended Reconstructed SST V5 (ERSSTv5) dataset (Huang *et al* 2017a), in a  $2^\circ \times 2^\circ$  grid and from 1854 to the present, provided by the National Oceanic and Atmospheric Administration (NOAA), United States. The Niño 3.4 index is the monthly SST anomaly from 1870 to the present and is based on the Hadley Centre Global Sea Ice and SST (HadISST) (Trenberth 1997). The Pacific Decadal Oscillation (PDO) index is the monthly SST anomaly over the North Pacific Ocean, from  $20^\circ$  N towards the pole, with data from 1854 to now, which is calculated with NOAA's ERSSTv5 (Mantua and Hare 2002).

Standardized Precipitation Evapotranspiration Index (SPEI) index is a standardized index widely used to describe drought conditions (Vicente-Serrano *et al* 2010). It is calculated by subtracting the accumulated precipitation over a 12 month period from the potential evapotranspiration (PET), and then standardizing the anomaly. The monthly SPEI data used in this study are derived from the SPEIbase dataset, version 2.9, in a  $0.5^\circ \times 0.5^\circ$  grid and from 1901 to 2022 (Beguería *et al* 2010).

### 2.2. Heatwave identification

The following heatwave occurrence criteria are established: (i) the daily maximum near-surface air temperature exceeds the  $35^\circ\text{C}$  threshold (You *et al* 2017); and (ii) an occurrence is considered a heatwave when the temperature exceeds the stated threshold for three or more consecutive days. In addition to heatwave days, to more effectively characterize the frequency, duration, and intensity of heatwaves, heatwave cumulative intensity (HWCI) has been established (Perkins-Kirkpatrick and Lewis 2020, Rousi *et al* 2022). HWCI is defined as the accumulated temperature exceeding the threshold during heatwave occurrences each year from May to September. The results of HWCI are largely consistent with those of heatwave days, including climatology, trends, standard deviation (figure S1), time series analysis of eastern and northern China, and key region analysis of decadal variability in relation to oceanic decadal variability (figure S2).

### 2.3. Temperature tendency equation

In order to provide a more detailed description of the effects of different physical processes on high temperatures, the model-level temperature tendency equation is employed:

$$\begin{aligned} \text{Local - tendency} &= \underbrace{-\vec{V} \cdot \nabla_h T}_{\text{Advection}} + \underbrace{\left( \frac{\kappa T}{p} \omega - \frac{\partial T}{\partial p} \omega_{\text{ml}} \right)}_{\text{Adiabatic}} \\ &+ \underbrace{\left( \frac{p}{p_0} \right)^\kappa \frac{d\theta}{dt}}_{\text{Diabatic}}, \end{aligned} \quad (1)$$

$$\omega_{\text{ml}} = \omega - \frac{\partial p}{\partial t} - \vec{V} \cdot \nabla_h p, \quad (2)$$

$$\frac{d\theta}{dt} = \frac{\partial \theta}{\partial t} + \vec{V} \cdot \nabla_h \theta + \omega_{\text{ml}} \frac{\partial \theta}{\partial p}, \quad (3)$$

where  $T$  denotes temperature and  $t$  represents time.  $p$  and  $p_0$  represent the pressure and a reference pressure, i.e. 1000 hPa, respectively.  $\vec{V}$  is the horizontal wind vector,  $\omega$  and  $\omega_{\text{ml}}$  vertical velocity in pressure and in model-level coordinates, respectively,  $\theta$  the potential temperature, where  $\omega_{\text{ml}}$  in equation (2) is obtained through the rules of vertical coordinate transformation (Xie *et al* 2022, 2023b).

The left-hand side of equation (1) contains the local-tendency term, whereas the right-hand

side contains the terms of temperature tendency due to horizontal temperature advection, adiabatic temperature modification, and diabatic heating or cooling-induced cold or warm temperature anomalies (Röthlisberger and Papritz 2023). The diabatic heating due to external energy input was calculated according to equation (3).

#### 2.4. Plumb wave activity flux

To investigate the pathway through which anomalous wave trains due to SST anomalies are transmitted to the eastern and northern parts of China, Plumb wave activity flux is employed (Plumb 1985), as follows:

$$F_s = \frac{p}{p_0} \cos \varphi \times \begin{pmatrix} v'^2 - \frac{1}{2\Omega a \sin 2\varphi} \frac{\partial(v'\phi')}{\partial \lambda} \\ -u'v' + \frac{1}{2\Omega a \sin 2\varphi} \frac{\partial(u'\phi')}{\partial \lambda} \\ \frac{f}{S} \left[ v'T' - \frac{1}{2\Omega a \sin 2\varphi} \frac{\partial(T'\phi')}{\partial \lambda} \right] \end{pmatrix}, \quad (4)$$

where  $\varphi$ ,  $\lambda$ , and  $\phi$  represent latitude, longitude, and geopotential, respectively.  $f = 2\Omega \sin \varphi$  denotes the Coriolis parameter.  $a$  and  $\Omega$  stand for the Earth's radius and rotational rate.  $p_0 = 1000$  hPa.  $u$  and  $v$  represent the zonal and meridional wind components. The prime symbol indicates the anomaly after removing the zonal mean value. First, the seasonal means of each variable are calculated for the months of May to September. Then, for the variables with primes, the zonal mean is removed.

#### 2.5. Decomposition of variables

In order to remove the interference of other oceanic variability when analyzing the influence of TSNAO and TIO SSTs, the study employed linear regression to decompose HWCI, SST, geopotential height, SPEI index, wave flux, and the terms (advective, adiabatic, and diabatic) from equation (1) into two parts: one is a linear regression associated with the oceanic variability to be excluded ( $R_p$ ), while the other is the residual of this linear regression, representing the independent portion ( $U_p$ ) (Li and Lu 2017, Liu *et al* 2020). In this way, the variables can be denoted as follows:

$$Var = R_p + U_p. \quad (5)$$

#### 2.6. Numerical simulations

In order to examine how the variations in the TSNAO and TIO SSTs individually contribute to the occurrence of heatwaves in China via atmospheric circulation patterns, we designed three sets of experiments using the Community Earth System Model (CESM) version 2.1.3 (table S1, Danabasoglu *et al* 2020): HIST as the control run, TSNAO-1K and TIO-1K as the sensitivity runs. The model is provided by the National Center for Atmospheric Research (NCAR)

and the University Corporation for Atmospheric Research (UCAR) in  $0.9^\circ \times 1.25^\circ$  grid and 32 vertical levels for the atmosphere component (table S1).

The three experiments were conducted from 1979 to 1994, as follows: The HIST experiment is consistent with the AMIP-historical experiment of the Coupled Model Inter-comparison Project Phase 6 (CMIP6, Eyring *et al* 2016); The TSNAO-1K and TIO-1K are based on HIST but with a 1K increase in the SSTs in TSNAO and TIO, respectively. The daily outputs were used to calculate heatwaves, while the monthly outputs were used for geopotential height.

#### 2.7. Statistical methods

The decadal components of HWCI, SST, and geopotential height were extracted using the Complete Ensemble Empirical Mode Decomposition with Adaptive Noise (CEEMDAN) approach (Torres *et al* 2011). The linear regression was employed to estimate the trend of climate variables and investigate the connections between the SSTs of TSNAO and TIO and other variabilities, including Plumb wave activity flux, various components of the temperature tendency equation. Its statistical significance is estimated using a two-tailed Student's t-test at a level of 0.05. The study confirmed the correlations between the SSTs of TSNAO and TIO and the HWCI in China using Pearson correlation analysis. The t-test for correlation coefficients is employed to determine the significance of the correlation at a level of 0.05.

### 3. Results

#### 3.1. Changes in heatwaves in China and the effect of oceanic variability

The HWCI in China from 1940 to 2022 was investigated using the given criteria. Two hot spots with frequent heatwaves are observed: one is the desert region of western China, where the partial cause of heatwaves is attributed to the semiarid and desert climates (Wu *et al* 2015); the other is the northern and eastern regions of China, with the average annual heatwave cumulative temperature being approximately  $8.5^\circ \text{C}$  per year in eastern China and  $4.3^\circ \text{C}$  in northern China (figure 1(a)). In addition to climatology, an analysis of the linear trends for the years 1940–2022 and the past ten years (2013–2022) and the standard deviation for the years 1940–2022 reveals that the occurrence of heatwaves is not uniformly increasing across China (figures 1(b)–(d)). For example, there was a significant decreasing trend of HWCI in the desert of western China, while HWCI increased in eastern China.

This study focuses on eastern and northern China due to the exceptionally high standard deviation from

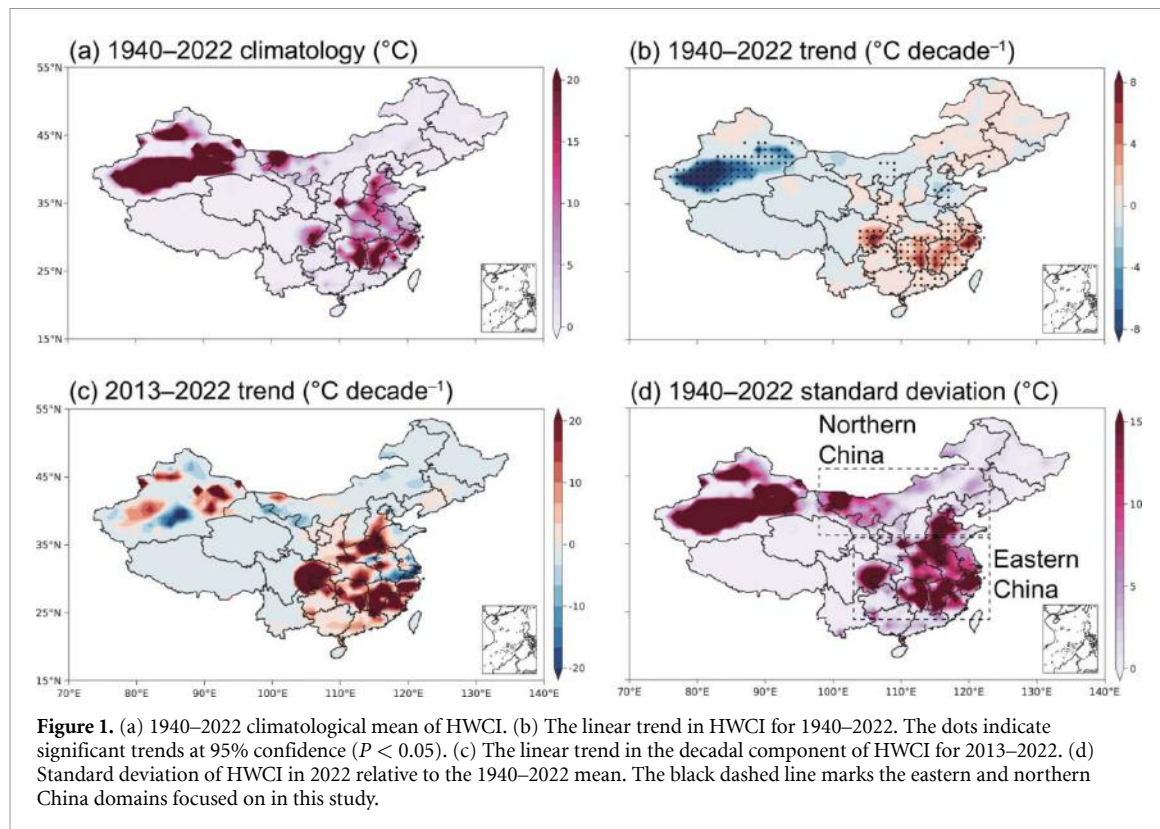


**Figure 1.** (a) 1940–2022 climatological mean of HWCI. (b) The linear trend in HWCI for 1940–2022. The dots indicate significant trends at 95% confidence ( $P < 0.05$ ). (c) The linear trend in the decadal component of HWCI for 2013–2022. (d) Standard deviation of HWCI in 2022 relative to the 1940–2022 mean. The black dashed line marks the eastern and northern China domains focused on in this study.

1940 to 2022 in eastern and northern China. The frequency decomposition of the time series of heatwaves in the eastern and northern regions of China based on the CEEMDAN is illustrated in figures 2 and S3. In figure 2(a), interannual component corresponds to Intrinsic Mode Function (IMF) 1, decadal component corresponds to IMF2–4, and long-term trend corresponds to IMF5 (figure S3). Averaged HWCI in eastern China increased with time from 1940 to 2022 (figure 2(a)). HWCI also showed significant interannual and decadal fluctuations (figures 2(a) and (b)). HWCI climbed dramatically for the eastern and northern China in the last decade, from 2013 to 2022. The long-term trend, interannual, and decadal components each contributed 6%, 24%, and 70%, respectively, to the  $15.9\text{ }^{\circ}\text{C}$  per-decade linear trend of HWCI in eastern China over the last decade. In northern China, the decadal component still exhibited a significant upward trend of  $3.4\text{ }^{\circ}\text{C}$  per decade, although the linear trend of HWCI over the past decade showed a decrease of  $-0.4\text{ }^{\circ}\text{C}$  per decade.

As a result, decadal component has dominated the current escalating heatwaves of the past decade in eastern and northern China. However, the contribution of the interannual component to the overall variance remains significant. Therefore, this study separately analyzes the interannual and decadal components of HWCI in eastern and northern China with respect to global SSTs. Compared to the decadal

component analysis, there is not a strong correlation between the two at the interannual component (figures 2(c), (d) and S4). Hence, this study primarily analyzes the influence of global SSTs on HWCI at the decadal component level.

After conducting a correlation analysis between decadal components of HWCI in eastern and northern China and global SSTs, a significant positive correlation is observed with the Pacific region, tropical Indian Ocean, and Atlantic (figures 2(c) and (d)). Although figures 2(c) and (d) indicate a prominent ENSO-like signal, the impact of Pacific SST on China is not discussed further due to the extensive existing research (Luo and Lau 2019, Tang *et al* 2023, Wei *et al* 2023). Instead, the focus is shifted to analyzing the influence of the Indian and Atlantic Oceans on heatwaves in eastern and northern China. Therefore, the study employed equation (5) to decompose HWCI, SST, geopotential height, SPEI index, Plumb wave activity flux, and the components (advective, adiabatic, and diabatic terms) from equation (1) into two parts: one linearly related to ENSO and the other unrelated to ENSO. Through this decomposition, it helps to partially isolate the ENSO signal to more focused examine the influence of TSNAO and TIO regional SSTs on heatwaves in China.

Due to the potential impact of local land-atmosphere exchanges on the occurrence of heatwaves (Sun *et al* 2021, Pan *et al* 2023), this study

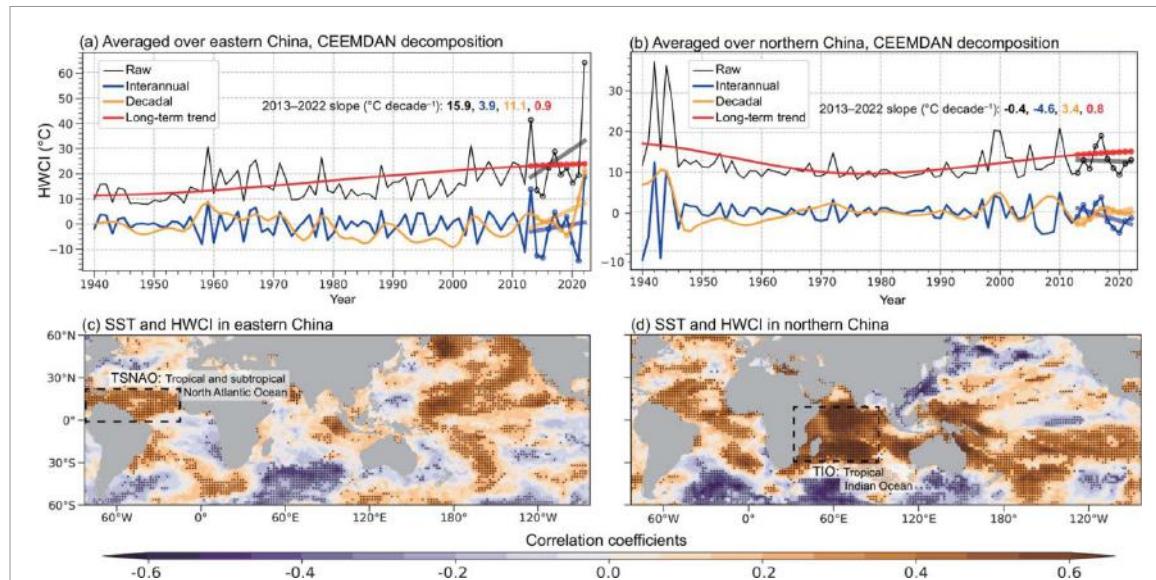


**Figure 2.** (a) Time series of HWCI averaged over eastern China, its interannual and decadal variability components, and long-term trend, based on CEEMDAN. The slopes of the linear fit for 2013–2022 are in units of  $^{\circ}\text{C decade}^{-1}$ . (c) Correlation coefficient between decadal variability components of the averaged HWCI in eastern China and SST. The dots indicate significant correlation at 95% confidence ( $P < 0.05$ ). (b), (d) Same as (a), (c) but for northern China. The black dashed line marks the TSNAO and TIO SSTs domains focused on in this study.

analyzed. The connection between the SPEI index from 1940–2022 in China. The climatology reveals a pronounced drought characteristic in the desert regions of western China (figure S5(a)). Moreover, examination of the linear trends for the years 1940–2022 and the past ten years (2013–2022) and standard deviation for the years 1940–2022 indicates that drought in various regions of China has not uniformly intensified. Among them, northern China exhibits the most pronounced strengthening of drought (figures S5(b)–(d)). Furthermore, the study conducted regional averages of the SPEI index corresponding to the same regions selected for HWCI. Correlation analysis of the decadal components of HWCI and SPEI showed a correlation of  $-0.4$  for eastern China and  $-0.6$  for northern China, both passing significance tests with  $P < 0.05$ . This observation underscores the significant role of drought in the occurrence of heatwaves.

### 3.2. Mechanisms underlying the influence of the Indian and Atlantic SSTs on heatwaves

The connection between the Indian and tropical Atlantic Oceans had been confirmed (Li *et al* 2016, Sun *et al* 2019). Hence, to mitigate the potential collinearity issues arising from the influence of the TSNAO and TIO SSTs on heatwaves in eastern and northern China, a diagnostic analysis employing multicollinearity was conducted. Since the variance inflation factor (VIF) for both regions remained below 5, with values of 1.063 219 for both the eastern and

northern China, there is no strong multicollinearity. However, to address the potential connection between the TSNAO and TIO SSTs, equation (5) was utilized to decompose HWCI, SST, geopotential height, SPEI index, wave flux, and the components (advective, adiabatic, and diabatic terms) from equation (2) in this study.

The dynamics underpinning the impact of TSNAO and TIO SSTs on heatwaves in China were examined further. The association between the averaged SSTs over the two regions and the decadal components of HWCI indicates that TSNAO and TIO SSTs have significant influences on the escalation of heatwave occurrences in the eastern and northern regions of China (figures 3(a) and (d)). The TSNAO exhibited a significant positive correlation with eastern China (figure 3(a)). And the TIO region showed a significant positive correlation with the northern region and a negative correlation with southern China (figure 3(d)). Additionally, Correlation analysis between the averaged SSTs over the two regions and the decadal components of the SPEI index reveals that drought significantly amplifies the impact of SST on the occurrence of heatwaves (figure S6).

Regarding the large-scale atmospheric circulation patterns, the TSNAO and TIO SSTs are positively correlated to the 500 hPa geopotential height (figures 3(b) and (e)) in regions with more heatwaves (figures 3(a) and (d)). More heatwaves are generally associated with high-pressure circulations. In specific, the TSNAO exhibited a significant positive correlation with eastern China, while a negative

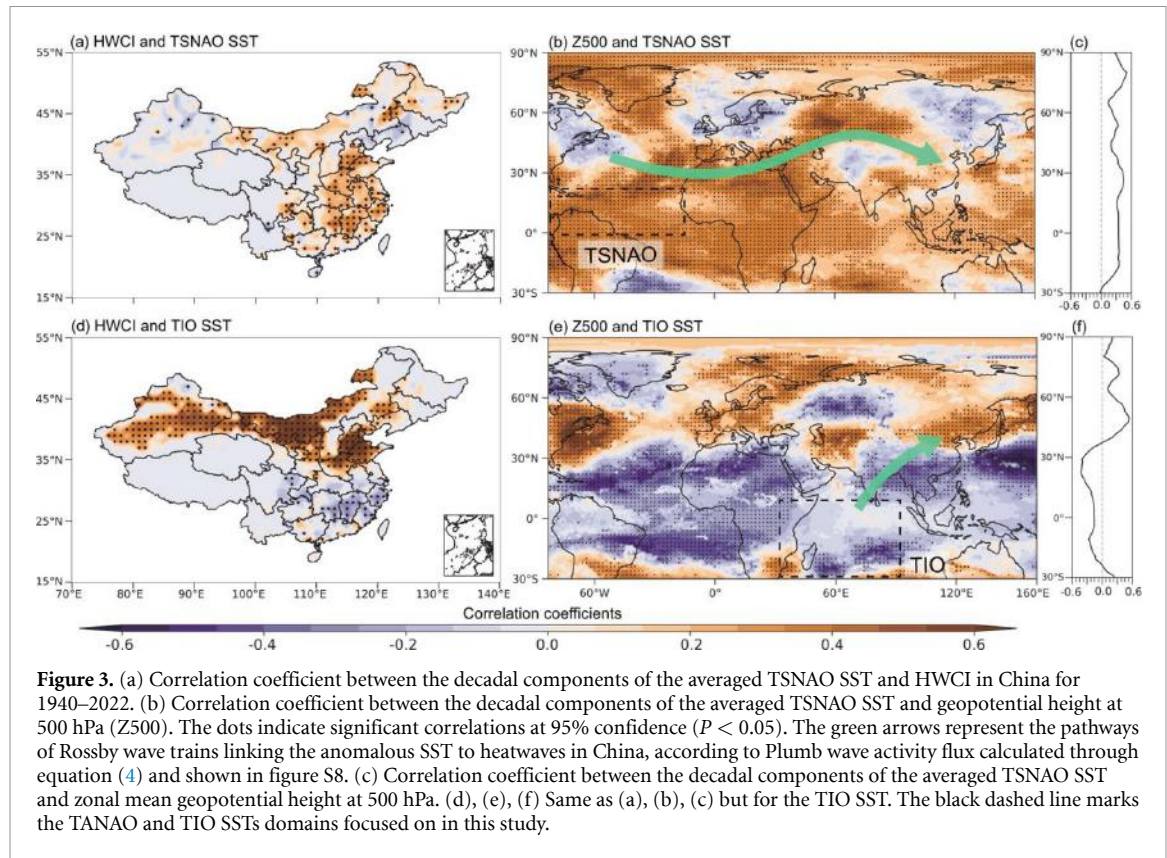


**Figure 3.** (a) Correlation coefficient between the decadal components of the averaged TSNAO SST and HWCI in China for 1940–2022. (b) Correlation coefficient between the decadal components of the averaged TSNAO SST and geopotential height at 500 hPa (Z500). The dots indicate significant correlations at 95% confidence ( $P < 0.05$ ). The green arrows represent the pathways of Rossby wave trains linking the anomalous SST to heatwaves in China, according to Plumb wave activity flux calculated through equation (4) and shown in figure S8. (c) Correlation coefficient between the decadal components of the averaged TSNAO SST and zonal mean geopotential height at 500 hPa. (d), (e), (f) Same as (a), (b), (c) but for the TIO SST. The black dashed line marks the TANAQ and TIO SSTs domains focused on in this study.

correlation was observed in the western region. And the TIO region showed a negative correlation with southern China and a significant positive correlation with the northern region. Therefore, the TSNAO and TIO SSTs have a remote influence on the heatwaves in China via abnormal atmospheric circulations.

The mutual impacts between TSNAO and TIO on the results were further analyzed. After excluding the influence of the TIO SST, the positive impact of the TSNAO SST on heatwaves in eastern China became more evident and in northern China significantly decreased (figures 3(a) and S7(a)), where the TSNAO SST showed a more positive influence on heatwaves in eastern and northern China when the TIO signature was removed (figures 3(d) and S7(c)). In contrast, after excluding the influence between TIO and TSNAO, the effect on geopotential height changed little (figures 3(b), (e) and S7(b), (d)), with only slight enhancements observed in the negative correlation in southern China and the positive correlation in northern China. The strong TIO SST signal is a result of the Walker circulation adjustment (Cai *et al* 2019) and downwelling Rossby wave in the south Indian Ocean (Xie *et al* 2002).

The TSNAO and TIO SSTs-induced positive geopotential height (figures 3(b) and (e)) and eddy streamfunction (figures S8(b) and (c)) anomalies in China are opposite to the negative eddy streamfunction center shown in the climatology (figure S8(a)). Additionally, the directions of the TSNAO and

TIO SSTs-induced anomalous wave activity flux are opposite to the climatological mean wave activity flux. Therefore, the warm anomalies of the TSNAO and TIO SSTs will induce the weakening of the climatological mean wave trains, while the cold SST anomalies will induce the strengthening of the climatological mean wave trains. The wave trains linked with TSNAO and TIO SSTs were marked in figures 3(b) and (e), respectively. The TSNAO-related wave trains originated from the north of TSNAO, passing through North Africa, Middle East, and Central Asia before reaching China (figure 3(b)). Regarding the TIO SST, the wave trains originated from the Indian Peninsula and subsequently reached the eastern and northern regions of China (figure 3(e)). The pathways of these wave trains were unchanged by the mutual impacts between TSNAO and TIO, although the magnitudes changed slightly (figures S8 and S9).

Moreover, the effect of the changes in mean circulation, i.e. westerlies, was greater than that of the waves associated with the atmospheric circulation affecting the heatwaves in China (figures 3(c), (f) and S8(b), (c)). Further analysis reveals the existence of a wave that encircles the globe along the jet stream. Therefore, the wave trains affected by TSNAO and TIO seem to be a subset of the circumglobal zonal wavenumber-4 pattern (Liu *et al* 2022, figure S10). In addition, the study examines the impact of the North Pacific SSTs, i.e. Pacific Decadal Oscillation (PDO), on the decadal component of

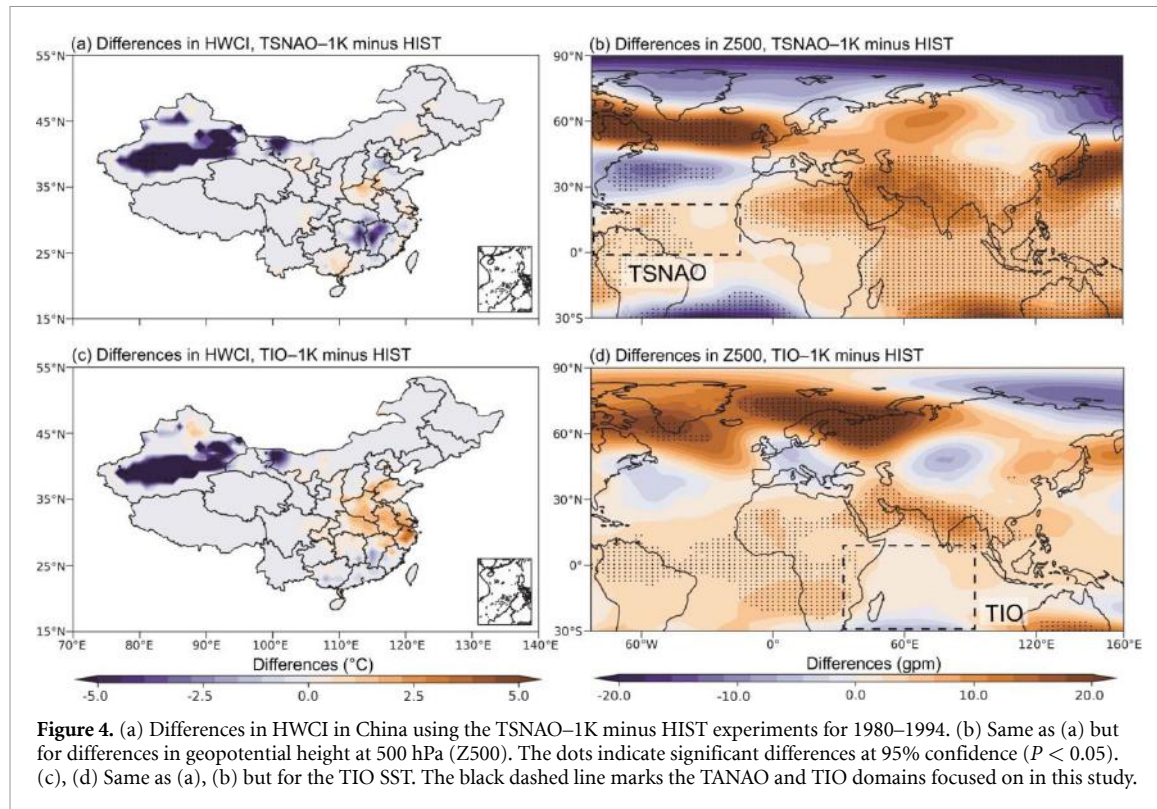


**Figure 4.** (a) Differences in HWCI in China using the TSNAO-1K minus HIST experiments for 1980–1994. (b) Same as (a) but for differences in geopotential height at 500 hPa (Z500). The dots indicate significant differences at 95% confidence ( $P < 0.05$ ). (c), (d) Same as (a), (b) but for the TIO SST. The black dashed line marks the TANAO and TIO domains focused on in this study.

HWCI in China (figure S11). The PDO exhibited a weak positive correlation with HWCI in eastern and northern China when the TIO and TSNAO signals were excluded. However, upon incorporating the signals from TIO and TSNAO, this positive correlation strengthened.

For a better examination of the individual impacts of TSNAO and TIO on heatwaves and atmospheric circulations in China, three sets of experiments were designed: HIST, TSNAO-1K, and TIO-1K. The spatial pattern of heatwaves simulated by the HIST experiment matched well with the ERA5 data, indicating a good performance of the model (figure S12). Subtracting HIST from TSNAO-1K and TIO-1K experiments represents the individual impacts of the TSNAO and TIO SSTs, respectively. The impact of the TSNAO and TIO SSTs on heatwaves in China exhibited certain disparities between modeling simulations and observations (figures 4(a) and (c)), whereas the circulation patterns and observations demonstrated a higher degree of consistency (figures 4(b) and (d)). Therefore, the impacts of the TSNAO and TIO SSTs on large-scale atmospheric circulations associated with heatwaves in China are robust. However, issues in modelling the process of circulation influencing heatwaves may stem from problems related to land-atmosphere feedback and the lack of fully active interaction between the ocean and atmosphere in our experiments, where only oceanic forcing is applied to the atmosphere.

To further investigate the physical processes underpinning heatwaves, the effects of the physical processes on SST-modulated temperature tendency in China were quantified according to equation (1). The magnitude of the residual term is one hundredth of the advective, adiabatic, and diabatic terms (figure S13), which indicates a good level of accuracy in the diagnostic procedure. In addition, the balance of the equation is between the advective, adiabatic, and diabatic terms because the local-tendency term is also one hundredth of the other terms. Therefore, the analysis focuses on the three physical processes, including horizontal temperature advection, vertical motion-induced adiabatic warming or cooling, and the diabatic heating effect owing to energy input.

For the effect of TSNAO SST, the adiabatic term played a strengthening role on heatwaves in the eastern and northern China (figures 5(c) and 3(a)). The diabatic term had a minor positive effect on heatwaves in eastern China and a minor negative effect in northern China (figure 5(e)). The advective term contributed negatively to heatwaves in eastern and northern China (figure 5(a)). For the effect of TIO SST, the diabatic term (figure 5(f)) had the dominant contribution to heatwaves in northern China (figure 3(d)). The adiabatic term (figure 5(d)) had a minor effect on heatwaves. The advective term contributed negatively to heatwaves in eastern and northern China (figure 5(b)).

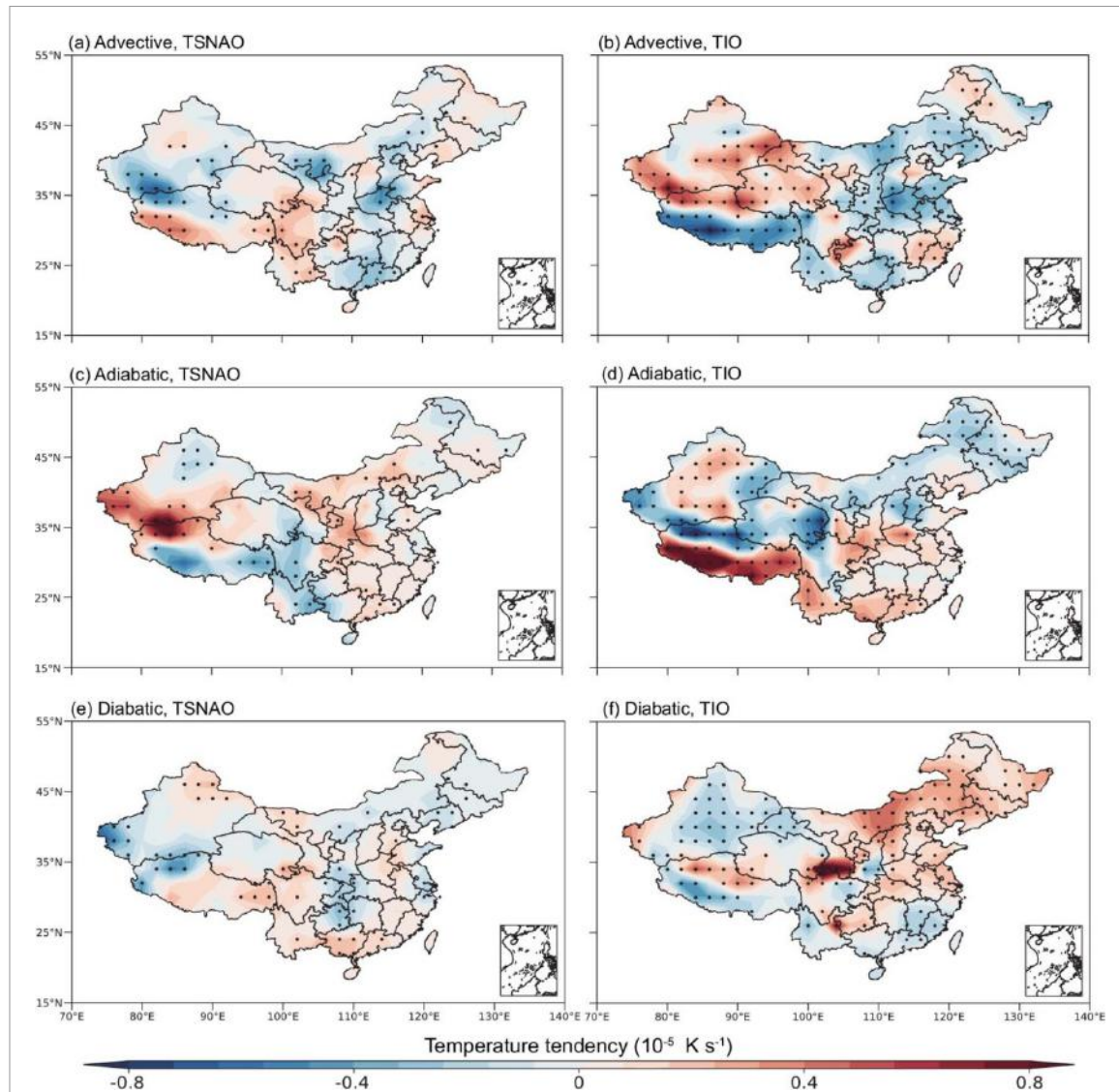


**Figure 5.** Linear regression analysis of the advective term, indicating the effect of horizontal temperature advection, in equation (1) with respect to the regional averaged (a) TSNAO and (b) TIO SSTs. (c), (d) And (e), (f) same as (a), (b) but for adiabatic and diabatic terms, which indicate the effects of vertical motion-induced adiabatic warming or cooling and the energy input-induced diabatic heating effect, respectively. The dots indicate significant differences at 95% confidence ( $P < 0.05$ ).

#### 4. Conclusions

In distinction to the widely recognized influence of interannual variability and ENSO (Deng *et al* 2019, Luo and Lau 2019, Tang *et al* 2023, Wei *et al* 2023), this study uncovers the crucial influence of decadal oceanic variability within the TSNAO and TIO SSTs on heatwaves in China. The study also establishes the dynamic and physical processes underpinning the remote influence of SSTs on heatwaves in China. In summary, TSNAO and TIO SSTs remotely influence heatwaves in China by stimulating anomalous westerlies and Rossby wave trains that zonally and northeasterly propagate from the north of TSNAO and the Indian Peninsula to China, respectively. The outcomes of the model simulations are consistent with the conclusions. In addition, the influence of TSNAO and TIO SSTs on heatwaves in China is determined by vertical motion-induced adiabatic and

energy input-induced diabatic temperature modification, with horizontal temperature advection playing a small role.

Meanwhile, the study has some shortcomings. For example, the influence of the ENSO signal was unable to be fully removed when using statistical methods to separate it out. Some of the ENSO signal's effects remained. In the process of conducting the simulation experiment, only the one-way effect of the ocean forcing the atmosphere was simulated, without utilizing the mutual interaction between the two, such as that in the peacemaker experiment (Kosaka and Xie 2013).

This study highlights the impact of decadal oceanic variability in the Atlantic and Indian Oceans on heatwaves in China. As a result, after excluding the influence of ENSO, SSTs in the two oceans should be considered while studying heatwaves in China. Furthermore, similar to ENSO, the TSNAO and TIO

SSTs may be employed to promote heatwave prediction in China. In terms of prediction, it should be examined further whether TSNAO and TIO SSTs have comparable predictability and persistence as ENSO.

## Data availability statement

All data and codes are publicly available. ERA5 data can be accessed at the ECMWF websites <https://cds.climate.copernicus.eu/cdsapp#!/dataset/reanalysis-era5-single-levels?tab=form>, <https://cds.climate.copernicus.eu/cdsapp#!/dataset/reanalysis-era5-pressure-levels-monthly-means?tab=form>, and <https://cds.climate.copernicus.eu/cdsapp#!/dataset/reanalysis-era5-complete?tab=form>. ERSSTv5 data can be accessed at [www.ncei.noaa.gov/products/extended-reconstructed-sst](http://www.ncei.noaa.gov/products/extended-reconstructed-sst). The PDO index can be accessed at [www.ncei.noaa.gov/pub/data/cmb/ersst/v5/index/ersst.v5.pdo.dat](http://www.ncei.noaa.gov/pub/data/cmb/ersst/v5/index/ersst.v5.pdo.dat). The ENSO index can be accessed at [https://psl.noaa.gov/gcos\\_wgsp/Timeseries/Data/nino34.long.data](https://psl.noaa.gov/gcos_wgsp/Timeseries/Data/nino34.long.data). The SPEIbase dataset can be accessed at <https://spei.csic.es/database.html>. The CESM outputs and codes for data processing and plotting are available at <https://zenodo.org/records/11178067>.

## Acknowledgments

We thank the anonymous reviewers for their constructive comments. We thank ECMWF and NOAA for making their data available. This work was supported by the National Key R & D Program of China (2023YFF0806700), the National Natural Science Foundation of China (91937302), the Fundamental Research Funds for the Central Universities (lzujbky-2022-kb10), and the Gansu Provincial Special Fund Project for Guiding Scientific and Technological Innovation and Development (2019ZX-06).

## ORCID iDs

Nan Lei  <https://orcid.org/0009-0009-3864-6804>  
 Yongkun Xie  <https://orcid.org/0000-0001-8836-9328>  
 Zifan Su  <https://orcid.org/0009-0006-5011-1202>  
 Xiaodan Guan  <https://orcid.org/0000-0003-3716-4503>

## References

Beguería S, Vicente-Serrano S M and Angulo-Martínez M 2010 A multiscalar global drought dataset: the SPEIbase: a new gridded product for the analysis of drought variability and impacts *Bull. Am. Meteorol. Soc.* **91** 1351–6

Cai W et al 2019 Pan tropical climate interactions *Science* **363** eaav4236

Cao D, Xu K, Huang Q, Tam C, Chen S, He Z and Wang W 2022 Exceptionally prolonged extreme heat waves over South China in early summer 2020: the role of warming in the tropical Indian Ocean *Atmos. Res.* **278** 106335

Chen R and Li X 2023 Causes of the persistent merging of the western North Pacific subtropical high and the Iran high during late July 2022 *Clim. Dyn.* **61** 2285–97

Choi N, Lee M I, Cha D H, Lim Y K and Kim K M 2020 Decadal changes in the interannual variability of heat waves in East Asia caused by atmospheric teleconnection changes *J. Clim.* **33** 1505–22

Danabasoglu G et al 2020 The Community Earth System Model Version 2 (CESM2) *J. Adv. Model. Earth Syst.* **12** e2019MS001916

Deng K, Yang S, Gu D, Lin A and Li C 2020 Record-breaking heat wave in southern China and delayed onset of South China Sea summer monsoon driven by the Pacific subtropical high *Clim. Dyn.* **54** 3751–64

Deng K, Yang S, Ting M, Zhao P and Wang Z 2019 Dominant modes of China summer heat waves driven by global sea surface temperature and atmospheric internal variability *J. Clim.* **32** 3761–75

Eyring V, Bony S, Meehl G A, Senior C A, Stevens B, Stouffer R J and Taylor K E 2016 Overview of the Coupled Model Intercomparison Project Phase 6 (CMIP6) experimental design and organization *Geosci. Model Dev.* **9** 1937–58

Fyfe J C et al 2016 Making sense of the early-2000s warming slowdown *Nat. Clim. Change* **6** 224–8

Guan X, Huang J, Guo R and Lin P 2015 The role of dynamically induced variability in the recent warming trend slowdown over the Northern Hemisphere *Sci. Rep.* **5** 12669

He C, Zhou T, Zhang L, Chen X and Zhang W 2023 Extremely hot East Asia and flooding western South Asia in the summer of 2022 tied to reversed flow over Tibetan Plateau *Clim. Dyn.* **61** 2103–19

Hersbach H et al 2020 The ERA5 global reanalysis *Q. J. R. Meteorol. Soc.* **146** 1999–2049

Huang B, Thorne P W, Banzon V F, Boyer T, Chepurin G, Lawrimore J H, Menne M J, Smith T M, Vose R S and Zhang H M 2017a Extended Reconstructed Sea Surface Temperature, Version 5 (ERSSTv5): upgrades, validations, and intercomparisons *J. Clim.* **30** 8179–205

Huang J, Xie Y, Guan X, Li D and Ji F 2017b The dynamics of the warming hiatus over the Northern Hemisphere *Clim. Dyn.* **48** 429–46

Jiang J, Liu Y, Mao J and Wu G 2023 Extreme heatwave over Eastern China in summer 2022: the role of three oceans and local soil moisture feedback *Environ. Res. Lett.* **18** 044025

Kosaka Y and Xie S 2013 Recent global-warming hiatus tied to equatorial Pacific surface cooling *Nature* **501** 403–7

Li J, Ding T, Jia X and Zhao X 2015 Analysis on the extreme heat wave over China around Yangtze River region in the summer of 2013 and its main contributing factors *Adv. Meteorol.* **2015** 706713

Li X and Lu R 2017 Extratropical factors affecting the variability in summer precipitation over the Yangtze River Basin, China *J. Clim.* **30** 8357–74

Li X, Xie S P, Gille S T and Yoo C 2016 Atlantic-induced pan-tropical climate change over the past three decades *Nat. Clim. Change* **6** 275–9

Liu Q, Zhou T, Mao H and Fu C 2019 Decadal variations in the relationship between the western Pacific subtropical high and summer heat waves in East China *J. Clim.* **32** 1627–40

Liu X, Liu Y, Wang X and Wu G 2020 Large-scale dynamics and moisture sources of the precipitation over the western Tibetan Plateau in boreal winter *J. Geophys. Res. Atmos.* **125** e2019JD032133

Liu Y, Sun C and Li J 2022 The boreal summer zonal wavenumber-3 trend pattern and its connection with surface enhanced warming *J. Clim.* **35** 833–50

Luo M and Lau N 2019 Amplifying effect of ENSO on heat waves in China *Clim. Dyn.* **52** 3277–89

Mantua N J and Hare S R 2002 The Pacific decadal oscillation *J. Oceanogr.* **58** 35–44

Pan X, Wang W, Shao Q, Wei J, Li H, Zhang F, Cao M and Yang L 2023 Compound drought and heat waves variation and association with SST modes across China *Sci. Total. Environ.* **907** 167934

Perkins-Kirkpatrick S E and Lewis S C 2020 Increasing trends in regional heatwaves *Nat. Commun.* **11** 3357

Plumb R A 1985 On the three-dimensional propagation of stationary waves *J. Atmos. Sci.* **42** 217–29

Röthlisberger M and Papritz L 2023 Quantifying the physical processes leading to atmospheric hot extremes at a global scale *Nat. Geosci.* **16** 210–6

Rousi E, Kornhuber K, Beobide-Arsuaga G, Luo F and Coumou D 2022 Accelerated western European heatwave trends linked to more-persistent double jets over Eurasia *Nat. Commun.* **13** 3851

Sun C, Li J, Kucharski F, Kang I S, Jin F F, Wang K, Wang C, Ding R and Xie F 2019 Recent acceleration of Arabian Sea warming induced by the Atlantic-western Pacific trans-basin multidecadal variability *Geophys. Res. Lett.* **46** 1662–71

Sun C, Zhu L, Liu Y, Hao Z and Zhang J 2021 Changes in the drought condition over northern East Asia and the connections with extreme temperature and precipitation indices *Glob. Planet. Change* **207** 103645

Sun J 2014 Record-breaking SST over mid-North Atlantic and extreme high temperature over the Jianghuai–Jiangnan region of China in 2013 *Sci. Bull.* **59** 3465–70

Sun Q, Miao C, AghaKouchak A and Duan Q 2017 Unraveling anthropogenic influence on the changing risk of heat waves in China *Geophys. Res. Lett.* **44** 5078–85

Tang S et al 2023 Linkages of unprecedented 2022 Yangtze River Valley heatwaves to Pakistan flood and triple-dip La Niña *npj Clim. Atmos. Sci.* **6** 44

Torres M E, Colominas M A, Schlotthauer G and Flandrin P 2011 A complete ensemble empirical mode decomposition with adaptive noise 2011 *IEEE Int. Conf. on Acoustics, Speech and Signal Processing (ICASSP)* pp 4144–7

Trenberth K E 1997 The definition of El Niño *Bull. Am. Meteorol. Soc.* **78** 2771–8

Vicente-Serrano S M, Beguería S and López-Moreno J I 2010 A multiscalar drought index sensitive to global warming: the standardized precipitation evapotranspiration index *J. Clim.* **23** 1696–718

Wang Z, Luo H and Yang S 2023 Different mechanisms for the extremely hot central-eastern China in July–August 2022 from a Eurasian large-scale circulation perspective *Environ. Res. Lett.* **18** 024023

Wei J, Han W, Wang W, Zhang L and Rajagopalan B 2023 Intensification of heatwaves in China in recent decades: roles of climate modes *npj Clim. Atmos. Sci.* **6** 98

Wei J, Wang W, Shao Q, Yu Z, Chen Z, Huang Y and Xing W 2020 Heat wave variations across China tied to global SST modes *J. Geophys. Res. Atmos.* **125** e2019JD031612

Wu Y, Bake B, Zhang J and Rasulov H 2015 Spatio-temporal patterns of drought in North Xinjiang, China, 1961–2012 based on meteorological drought index *J. Arid Land* **7** 527–43

Xie S, Annamalai H, Schott A and McCreary J 2002 Structure and mechanisms of south Indian Ocean climate variability *J. Clim.* **15** 864–78

Xie T, Wang J, Feng T, Ding T and Zhao L 2023a Linkage of the decadal variability of extreme summer heat in North China with the IPOD since 1981 *Adv. Atmos. Sci.* **40** 1617–31

Xie Y, Wu G, Liu Y, Huang J and Nie H 2022 A dynamic and thermodynamic coupling view of the linkages between Eurasian cooling and Arctic warming *Clim. Dyn.* **58** 2725–44

Xie Y, Wu G, Liu Y, Huang J, Sheng C and Wu Y 2023b A potential vorticity budget view of the atmospheric circulation climatology over the Tibetan Plateau *Int. J. Climatol.* **43** 2031–49

You Q, Jiang Z, Kong L, Wu Z, Bao Y, Kang S and Pepin N 2017 A comparison of heat wave climatologies and trends in China based on multiple definitions *Clim. Dyn.* **48** 3975–89

Zhang D, Chen L, Yuan Y, Zuo J and Ke Z 2023 Why was the heat wave in the Yangtze River valley abnormally intensified in late summer 2022? *Environ. Res. Lett.* **18** 034014